International Journal of Heat and Mass Transfer 52 (2009) 173–180

Contents lists available at ScienceDirect

International Journal of Heat and Mass Transfer

journal homepage: www.elsevier.com/locate/ijhmt

Simulation of one method of laser welding of metal plates involving an SHS-reacting powder mixture

V.V. Belyaev *, O.B. Kovalev

Khristianovich's Institute of Theoretical and Applied Mechanics, SB RAS, Institutskaja Str., 4/1, Novosibirsk 630090, Russia

ARTICLE INFO

Article history:
Received 23 January 2008
Received in revised form 12 May 2008
Available online 4 August 2008

Keywords:
Self-propagating high-temperature synthesis
Laser radiation
Fuse welding
Aluminum
Titanium
Mathematical simulation

ABSTRACT

The mathematical model is based on the physical and chemical mechanism of the fusion penetration of welded joints involving the energy of chemical interaction in a powder mixture in the self-propagating high-temperature synthesis (SHS) mode. The reacting mixture located inside the joint between thermal-conducting metal plates is initiated with a laser beam moving simultaneously along the plate contact boundary. The minimum power of the laser radiation and physical and chemical properties of the powder mixture needed to provide the sufficient velocity of the welding and depth of plate joint penetration have been determined. Numerical simulation has enabled to ground theoretically the possibility of realization of the SHS welding of both homogeneous and heterogeneous plates from aluminum and titanium with no steam–gas channel in the stable mode, when the intrinsic velocity of the SHS propagation does not exceed the welding velocity.

1. Introduction

The self-propagating high-temperature synthesis (SHS) is applied to weld refractory and heterogeneous metals; the welding is carried out due to the exothermic interaction between the components of the reaction mixture located in the clearance between the jointed materials [1–4]. The reaction mixture can contain metal and non-metal powders forming carbides, borides, silicides, intermetallides and other compounds.

Synthesis reactions are normally initiated either through the local thermal action followed by the propagation over the whole mixture in the self-maintaining mode [1,2], or due to the electric-thermal explosion, when the reacting mixture is heated together with the units to be connected up to the temperature at which all reagents begin to interact in the whole mixture simultaneously [1–4]. In both cases, a large amount of heat is released.

The formed high-temperature region of the SHS products fuses the surfaces of the jointed materials. During the welding, material synthesis and welded joint are carried out simultaneously.

The main advantages of the method are: high heat release, high heating and cooling rates. Now almost any methods of heterogeneous metal welding involve the increased pressure, and only the SHS-method permits to weld at atmospheric pressure [4].

Among the disadvantages of the SHS-method, there is impossibility to control the processes because of the physical parameters variety and no agreement in their choice, and also the need to heat the connected units up to the temperature of the reaction start, which inevitable results in permanent strains of the whole construction after cooling.

The method of laser SHS welding of the materials [5] is based on the local dynamic laser heating and initiation of SHS reactions directly in the clearance between the connected plates. Reaction initiation is carried out on the joint surface in the region of action of the laser beam moving with the constant velocity. The fusion steadiness in the joint region and welding quality are guaranteed by the thermal balance, which is constituted by a heat flux applied by the radiation, heat release directly in the reacting mixture, and heat consumption due to the thermal conductivity of the metal. The thermal balance is provided by the agreement between the speed of propagation of the SHS reactions and welding rate. Welding energy is considerably provided by the exothermic SHS reactions, laser radiation may be just auxiliary.

The practical realization of the laser SHS welding is difficult because of the absence of stable initiation of the chemical SHS reactions and its propagation in the narrow clearance between the thermal-conducting plates.

The development of this method is restrained by the absence of proper techniques of simulation and calculation in the conjugate tasks of heat- and mass-exchange and heat- and mass transfer during the laser SHS welding.

* Corresponding author. Tel.: +7 383 330 42 73; fax: +7 383 330 72 68.
E-mail address: belyaev@itam.nsc.ru (V.V. Belyaev).

0017-9310/$ - see front matter © 2008 Elsevier Ltd. All rights reserved.
doi:10.1016/j.ijheatmasstransfer.2008.05.026

Nomenclature

A	absorption factor
c	specific heat
d	metal plate thickness
E_a	activation energy
$f(t,x,y)$	phase transition surface
H	latent heat of the phase transition
I	density of radiation intensity
k_p	pre-exponential factor
L_x, L_y	sizes of the calculation domain by the coordinates x, y
$\vec{n}$	surface normal vector
Nu	Nusselt number
p	reaction order
Q_c	heat effect of SHS reactions
R	gas constant
r	half-width of the clearance filled with the combustible mixture
T	temperature
T_m	melting temperature
T_0	initial temperature
t	time
V_w	velocity of beam motion (welding rate)
W	radiation power
x, y, z	Cartesian coordinates
α	angle of joint surface deviation from the vertical
β	coefficient of the plate and ambient heat exchange
γ	angle of incidence
Δ	temperature interval of the numerical approximation of the Dirac's δ-function in the fusion point
δ	clearance gap between the plate and substrate
ε	emissivity
λ	thermal conductivity
ρ	density
η	substance transformation degree
σ	Stefan–Boltzmann constant
ω_0	laser beam radius in the focal plane
Ω	sub-region

Sub-indices

air	air
s	solid phase
m	liquid phase

The simulation of these processes permits to calculate the optimum fuse welding modes, to predict the values of such physical parameters as radiation power, rate of beam scanning, beam sizes, and also the physical and chemical properties of the reacting powder mixture.

General SHS theory and practice have been developed in a number of fundamental works [6–12]. Multidimensional numerical simulation of the SHS processes permits to study the mechanisms of the layer propagation of a gas-free flame [6,11] and spin combustion [6,8,9], as well as to investigate the peculiarities of the thermal explosion of the powder mixture [10,12]. The results of above fundamental researches have are commonly used in various applied tasks. One such task involving the methods of SHS [6,8,9] description has been considered in this paper.

The paper is devoted to the study of peculiarities of interacting laser radiation and reacting mixture under the conditions of intensive heat sink from the reaction area. Experimental and calculation findings of other authors within these themes, which would directly refer to the laser SHS welding, remain unknown for the authors of this paper.

The present work offers the mathematical statement of the problem and results of numerical simulation of the welding of both homogeneous aluminum and titanium plates and heterogeneous metals – titanium and aluminum.

2. Problem statement

The problem of interaction between the laser radiation and metals is difficult because of the variety of the physical processes, which cannot be described in details at the moment. The present problem statement is based on the following assumptions.

- The used density of the laser radiation power does not exceed 10^5 W/(cm^2), so it is assumed that the energy of the absorbed radiation is consumed only for the metal heating and fusing. The effects of evaporation and interaction between radiation and metal vapors are beyond our consideration.
- Due to weak power of the used radiation, with no external dynamic action, the convective motion in the liquid medium is neglected; this motion may appear owing to the thermocapillary convection or pressure. So, the hydrodynamic phenomena in the welding area are neglected too.
- Radiation heat losses and heat exchange with the ambient and substrate material, on which the welded plates are set, are taken into account.
- The material of the jointed plates and powder mixture are isotropic and possess homogeneous thermophysical properties in solid and liquid states.

Fig. 1 shows the layout of the fusion welding, when the mixture of reacting powders is set in the clearance between the jointed plates. The arrows show the direction of radiation action, which heats locally the material and initiates the SHS reactions. Let us designate the sub-region occupied with the powder mixture as Ω_1, and the sub-regions occupied with the metal as Ω_2 and Ω_3:

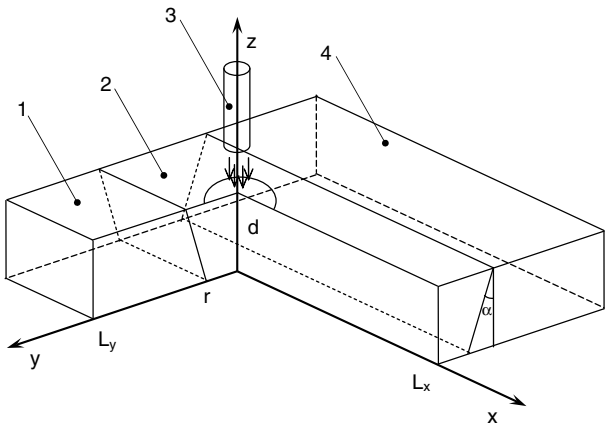

Fig. 1. Welding layout. 1, 4, Metal plates; 2, powder; 3, laser beam.

$$\Omega_1 = \{x,y,z : -L_x \leqslant x \leqslant L_x, \quad -r - z\cdot tg\alpha \leqslant y \leqslant r + z\cdot tg\alpha, \quad 0 \leqslant z \leqslant d\},$$
$$\Omega_2 = \{x,y,z : -L_x \leqslant x \leqslant L_x, \quad r + z\cdot tg\alpha \leqslant y \leqslant L_y,\ 0 \leqslant z \leqslant d\},$$
$$\Omega_3 = \{x,y,z : -L_x \leqslant x \leqslant L_x, \quad -L_y \leqslant y \leqslant -r - z\cdot tg\alpha,\ 0 \leqslant z \leqslant d\},$$

where L_x, L_y are the sizes of the region by the coordinates x, y; r – the half-width of the clearance which is filled with the combustible mixture; d – the thickness of the metal plates; α – the angle of joint surface deviation from the vertical.

The mathematical problem definition is reduced to the consideration in the conjugate definition of the processes of powder mixture ignition and combustion in the clearance, with the simultaneous heating and melting of the plate's metal. Let us consider the moving coordinates associated with the laser beam moving along the OX axis with the velocity of V_w, Fig. 1.

The thermal theory of SHS is used to describe the combustion of the reacting mixture in the region Ω_1; this theory is based on the formally kinetic approach [6,8,9]:

$$c_1\rho_1\left(\frac{\partial T_1}{\partial t} - V_w\frac{\partial T_1}{\partial x}\right) = \frac{\partial}{\partial x}\lambda_1\frac{\partial T_1}{\partial x} + \frac{\partial}{\partial y}\lambda_1\frac{\partial T_1}{\partial y} + \frac{\partial}{\partial z}\lambda_1\frac{\partial T_1}{\partial z} + Q_c\frac{\partial \eta_1}{\partial t}, \tag{1}$$

$$\frac{\partial \eta_1}{\partial t} - V_w\frac{\partial \eta_1}{\partial x} = k_p(1-\eta_1)^p \exp\left(-\frac{E_a}{RT_1}\right), \tag{2}$$

where t – time, x, y, z – the coordinates, $T_1(t,x,y,z)$ – the temperature in Ω_1, η_1 (t,x,y,z) – the degree of substance transformation into Ω_1, ρ_{1s}, λ_{1s}, c_{1s} and ρ_{1m}, λ_{1m}, c_{1m} – the density, thermal conductivity and specific heat of the powder mixture in the solid (s) and liquid (m) phases, correspondingly, V_w – the beam motion velocity (or welding rate), Q_c – thermal effect of the SHS reactions, k_p – pre-exponential multiplier, p – reaction order, E_a – activation energy, R – gas constant.

Thermal SHS theory (1), (2) suggests that the thermophysical properties of the initial powder and product mixture differ slightly, that is why we consider the values of density ρ_1, thermal conductivity λ_1, and heat capacity c_1 mean for the mixture. The model (1), (2) has shown itself when solving a number of practical tasks [6]. In particular, this model was used to research successfully the peculiarities of combustion of industrial pyrotechnical compositions under the conditions of the intensive heat sink [13].

Heat propagation in the metal, metal heating and fusion in the regions Ω_2 and Ω_3 are described with the two-phase Stefan's problem:

$$c_i\rho_i\left(\frac{\partial T_i}{\partial t} - V_w\frac{\partial T_i}{\partial x}\right) = \frac{\partial}{\partial x}\lambda_i\frac{\partial T_i}{\partial x} + \frac{\partial}{\partial y}\lambda_i\frac{\partial T_i}{\partial y} + \frac{\partial}{\partial z}\lambda_i\frac{\partial T_i}{\partial z}, \tag{3}$$

$$\rho_{im}H_i\left(\frac{\partial f_i}{\partial t} - V_w\frac{\partial f_i}{\partial x}\right) = \lambda_{is}\frac{\partial T_i}{\partial \vec{n}}\bigg|_{z=f_i(t,x,y)-0} - \lambda_{im}\frac{\partial T_i}{\partial \vec{n}}\bigg|_{z=f_i(t,x,y)+0}, \tag{4}$$

$$T_i(t,x,y,f_i(t,x,y)-0) = T_i(t,x,y,f_i(t,x,y)+0) = T_{im}, \tag{5}$$

where $T_i(t,x,y,z)$ – the temperature in Ω_i, $z = f_i(t,x,y)$ – phase transition surface, $\vec{n}$ – normal to this surface, ρ_i, λ_i, c_i – the density, thermal conductivity and specific heat of the metal, H_i – latent heat of the phase transition, $i = 2, 3$.

Initial conditions. It is assumed that before the beginning of radiation action the powder mixture and metal plate have the constant temperature, i.e. at the initial time moment:

$$T_1(0,x,y,z) = T_2(0,x,y,z) = T_3(0,x,y,z) = T_0, \quad \eta_1(0,x,y,z) = 0. \tag{6}$$

Boundary conditions. At any time moment, the following conditions are satisfied on the region boundaries:

$$x = \pm L_x,\ -r - z\cdot tg\alpha \leqslant y \leqslant r + z\cdot tg\alpha,\ 0 \leqslant z \leqslant d:\ \frac{\partial T_1}{\partial x} = 0, \tag{7}$$

$$x = \pm L_x,\ r + z\cdot tg\alpha < y \leqslant L_y,\ 0 \leqslant z \leqslant d:\ \frac{\partial T_2}{\partial x} = 0, \tag{8}$$

$$x = \pm L_x,\ -L_y \leqslant y < -r - z\cdot tg\alpha,\ 0 \leqslant z \leqslant d:\ \frac{\partial T_3}{\partial x} = 0, \tag{9}$$

$$y = r + z\cdot tg\alpha,\ -L_x \leqslant x \leqslant L_x,\ 0 \leqslant z \leqslant d:\ \lambda_1\frac{\partial T_1}{\partial y} = \lambda_2\frac{\partial T_2}{\partial y}, \tag{10}$$

$$y = -r - z\cdot tg\alpha,\ -L_x \leqslant x \leqslant L_x,\ 0 \leqslant z \leqslant d:\ \lambda_1\frac{\partial T_1}{\partial y} = \lambda_3\frac{\partial T_3}{\partial y}, \tag{11}$$

$$y = L_y,\ -L_x \leqslant x \leqslant L_x,\ 0 \leqslant z \leqslant d:\ \frac{\partial T_2}{\partial y} = 0, \tag{12}$$

$$y = -L_y,\ -L_x \leqslant x \leqslant L_x,\ 0 \leqslant z \leqslant d:\ \frac{\partial T_3}{\partial y} = 0. \tag{13}$$

At $z = 0$, $-L_x \leqslant x \leqslant L_x$:

$$-r - z\cdot tg\alpha \leqslant y \leqslant r + z\cdot tg\alpha,\ -\lambda_1\frac{\partial T_1}{\partial z} = \frac{\lambda_{air}}{\delta}(T_0 - T_1), \tag{14}$$

$$r + z\cdot tg\alpha < y \leqslant L_y,\ -\lambda_2\frac{\partial T_2}{\partial z} = \frac{\lambda_{air}}{\delta}(T_0 - T_2), \tag{15}$$

$$-L_y \leqslant y < -r - z\cdot tg\alpha,\ -\lambda_3\frac{\partial T_3}{\partial z} = \frac{\lambda_{air}}{\delta}(T_0 - T_3). \tag{16}$$

At $z = d$, $-L_x \leqslant x \leqslant L_x$:

$$-r - z\cdot tg\alpha \leqslant y \leqslant r + z\cdot tg\alpha,\ \lambda_1\frac{\partial T_1}{\partial z} = A(\gamma)I(x,y)\cos\gamma - \beta(T_1 - T_0) - \varepsilon\sigma(T_1^4 - T_0^4), \tag{17}$$

$$r + z\cdot tg\alpha \leqslant y \leqslant L_y,\ \lambda_2\frac{\partial T_2}{\partial z} = A(\gamma)I(x,y)\cos\gamma - \beta(T_2 - T_0) - \varepsilon\sigma(T_2^4 - T_0^4), \tag{18}$$

$$-L_y \leqslant y \leqslant -r - z\cdot tg\alpha,\ \lambda_3\frac{\partial T_3}{\partial z} = A(\gamma)I(x,y)\cos\gamma - \beta(T_3 - T_0) - \varepsilon\sigma(T_3^4 - T_0^4), \tag{19}$$

where $I(x,y)$ – the radiation intensity density, $A(\gamma)$ – absorption factor, γ – the angle of incidence, $\beta = \frac{Nu\lambda_{air}}{2\omega_0}$ – the heat-exchange coefficient between the heated section of the plate and ambient.

The sizes of the calculation domain L_x, L_y were chosen in such a way to exclude the influence of the boundaries over the length and width of the welded plates. Thus, Eqs. (7)–(9), (12), (13) describe the thermoisolation conditions on the corresponding boundaries of the calculation domain.

The conjunction conditions (10), (11) describe the heat exchange between the powder and metal on the interface. Their validity is based on the assumption of homogeneous physical properties of the contacting media.

Eqs. (14)–(16) describe the heat exchange between the heated plates and cold substrate. The plates and substrate contact is suggested to be non-ideal. We assume that there is an air space between the plate and substrate, its thickness is δ. Here, λ_{air} – the thermal conductivity of the ambient air in normal conditions; T_0 – the substrate's temperature equal to the ambient temperature.

Eqs. (17)–(19) are the conditions on the top surface of the plates where the laser radiation acts. The first term in the right part regards the laser radiation absorption by the combustible mixture and metal itself, two other terms account the heat losses from the heated surface resulting from the heat sink into the ambient and radiation heat losses. Here, Nu – the Nusselt number; ε – emissivity; σ – Stefan–Boltzmann constant.

The continuously acting radiation of the CI_2-laser is under consideration. Its intensity density is described with the Gaussian's distribution:

$$I(x,y) = \frac{2W}{\pi\omega_0^2}\exp\left\{-\frac{2(x^2+y^2)}{\omega_0^2}\right\},$$

where W – the radiation power, ω_0 – beam radius in the focal plane.

The variation of heat capacity factor, density and thermal conductivity regarding the temperature in the phase-transition region are taken into account. It is assumed that on the phase-transition boundary at $T_i(t,x,y,z) = T_{im}$, $i = 2, 3$, the density and thermal conductivity undergo a step rise, and the heat capacity is described with the aid of the Dirac's δ-function [6].

Existing effective algorithms of the numerical solution of the two-phase Stefan's problem are based on the technique of enthalpy jump or transport factors smoothing in the thermal-conductivity equation, in the fusion point [14–16], and also on the solution of the thermal-conductivity equation in the enthalpy onset [17]. Given techniques allow performing the shock-capturing calculations, i.e. with no explicit segregation of the melting front. Taking the differences in thermophysical properties of the contacting media (powder and metal), let us consider the auxiliary problem in the region of $\Omega_1 \cup \Omega_2 \cup \Omega_3$ with the variable coefficients in the thermal conductivity equation.

$$c\rho\left(\frac{\partial T}{\partial t} - V_w\frac{\partial T}{\partial x}\right) = \frac{\partial}{\partial x}\lambda\frac{\partial T}{\partial x} + \frac{\partial}{\partial y}\lambda\frac{\partial T}{\partial y} + \frac{\partial T}{\partial z}\lambda\frac{\partial T}{\partial z} + Q_c\frac{\partial \eta}{\partial t}, \tag{20}$$

$$\frac{\partial \eta}{\partial t} - V_w\frac{\partial \eta}{\partial x} = k_p(1-\eta)^p \exp\left(-\frac{E_a}{RT}\right). \tag{21}$$

Here, the sought functions and transport factors are defined over the whole region of $\Omega_1 \cup \Omega_2 \cup \Omega_3$:

$$T(t,x,y,z) = \begin{cases} T_1(t,x,y,z), & x,y,z \in \Omega_1 \\ T_2(t,x,y,z), & x,y,z \in \Omega_2 \\ T_3(t,x,y,z), & x,y,z \in \Omega_3 \end{cases},$$

$$\eta(t,x,y,z) = \begin{cases} \eta_1(t,x,y,z), & x,y,z \in \Omega_1 \\ 1, & x,y,z \in \Omega_2 \cup \Omega_3 \end{cases}$$

$$c\rho = \begin{cases} (1-\eta)c_{1s}\rho_{1s} + \eta c_{1m}\rho_{1m}, & x,y,z \in \Omega_1 \\ (c\rho)_2(T), & x,y,z \in \Omega_2 \\ (c\rho)_3(T), & x,y,z \in \Omega_3 \end{cases}$$

$$(c\rho)_i(T) = \begin{cases} c_{is}\rho_{is}, & T - T_{im} \leqslant -\Delta \\ 0.5(c_{is}\rho_{is} + c_{im}\rho_{im}) + \frac{\rho_{im}H_i}{2\Delta}, & |T - T_{im}| < 2\Delta \\ c_{im}\rho_{im}, & T - T_{im} \geqslant \Delta \end{cases},$$

$$\lambda(t,x,y,z) = \begin{cases} (1-\eta)\lambda_{1s} + \eta\lambda_{1m}, & x,y,z \in \Omega_1 \\ \lambda_2(T), & x,y,z \in \Omega_2 \\ \lambda_3(T), & x,y,z \in \Omega_3 \end{cases},$$

$$\lambda_i(T) = \begin{cases} \lambda_{is}, & T - T_{im} \leqslant -\Delta \\ 0.5(\lambda_{is} + \lambda_{im}), & |T - T_{im}| < 2\Delta \\ \lambda_{im}, & T - T_{im} \geqslant \Delta \end{cases}$$

$i = 2, 3.$

Boundary conditions.

$$x = \pm L_x,\ 0 < y \leqslant L_y,\ 0 \leqslant z \leqslant d:\ \frac{\partial T}{\partial x} = 0, \tag{22}$$

$$y = 0,\ -L_x \leqslant x \leqslant L_x,\ 0 \leqslant z \leqslant d:\ \frac{\partial T}{\partial y} = 0, \tag{23}$$

$$y = L_y,\ -L_x \leqslant x \leqslant L_x,\ 0 \leqslant z \leqslant d:\ \frac{\partial T}{\partial y} = 0, \tag{24}$$

$$z = 0,\ -L_x \leqslant x \leqslant L_x,\ 0 < y \leqslant L_y,\ -\lambda\frac{\partial T}{\partial z} = \frac{\lambda_{air}}{\delta}(T_0 - T), \tag{25}$$

$$z = d,\ -L_x \leqslant x \leqslant L_x,\ 0 < y \leqslant L_y,\ \lambda\frac{\partial T}{\partial z} = A(\gamma)I(x,y)\cos\gamma - \beta(T - T_0) - \varepsilon\sigma(T^4 - T_0^4). \tag{26}$$

Eqs. (20), (21) with the initial (6) and boundary conditions (22)–(26) were solved numerically on a non-uniform mesh, using the explicit differential scheme with coefficients smoothing [15]. In the calculation domain points, the mesh pitches by the coordinates x, y were increased to reduce the total amount of mesh nodes and calculation volume. The reliability of the presented results has been repeatedly proven by the calculations wherein the mesh pitches were reduces to the values when the temperature fields did not change anymore.

The problem was solved by the pseudoviscosity method; according to this method the numerical solution must be reduced to the precise one, when the time t infinitely rises. Realized numerical method is described in more details in [5].

3. Calculation results and discussion

3.1. Purposes of calculations and initial data

The mathematical model and solution method offered above are purposed to carry out numerical experiments and to optimize the physical parameters of the problem. It is necessary, with the assigned metal thickness and velocity of beam motion, to obtain the stable modes of combustion of the reacting mixture and hence to provide the fusion zone of sufficient size, which, upon cooling down, forms the welded joint.

The regularity of SHS initiation and combustion front propagation were studied in a number of papers which are reviewed in [6,7,11]. The SHS is referred to the intractable initiated combustion processes. With the assigned power of the sample cylindrical heat flux locally applied to the end-face surface, there is the delay time and ignition temperature, which starts the gas-free combustion. Upon the initiation, a certain mode of the combustion propagation is set; it features the linear velocity of the front motion, maximum combustion temperature and substance transformation degree. For the cylindrical samples, the stationary mode realizes in the most cases, the combustion rate here is constant. It is known, however, that the combustion rate depends on a number of physical parameters (initial temperature of the sample, its diameter, porosity, composition and dispersity of the powder mixture), and that non-stationary unstable modes may appear on the combustion limit, up to combustion termination [6,7,11]. Mathematical simulation of the processes of SHS initiation and propagation in 1D statement were studied in [11].

The purpose of these calculations is to produce stable stationary modes of combustion of the reacting mixture in the clearance, providing the full fusion of the joint of welded metal plates on the boundary of the contact with the combustible mixture.

In the calculations, the following initial data were used: the factor of radiation absorption by the powder mixture $A(\gamma) = 0.14$, initial temperature $T_0 = 300$ K, welding rate or the velocity of beam scanning along the plates joint $V_w = 0.12$ m/s. The thermophysical properties of the materials are given in Table 1.

Kinetics of the chemical reactions of the high-temperature synthesis of the powder mixture has been chosen from the analyzed results of the experimental investigations reviewed in [6,7]: $Q_c = 13.125 \times 10^9$ J/m^3, $k_p = 1.51 \times 10^6$ kg/(s m^3), $p = 0.8$, $E_a = 34$ kJ/mol.

The calculation experiments were performed, wherein the physical parameters of the problem were varied within the wide range – for example, the half-width of the clearance r, where the reacting mixture is found, its thermophysical and physical and chemical properties, the beam motion velocity, beam diameter, etc. The temperature interval $\Delta = 50$–100 K is conditioned by the extension of a δ-function maximum on 2–4 calculation cells.

3.2. Aluminum plates welding

When homogeneous plates are connected, the problem is symmetrical relative to the axial plane XZ, that is why only the half of

Table 1
Thermophysical properties of the materials

Material	Density (g/cm^3)	Heat capacity (J/(kg K))	Thermal conductivity (J/(m s K))	Melting temperature (K)	Melting heat (kJ/kg)
	ρ_s/ρ_m	c_s/c_m	λ_s/λ_m	T_m	H_m
Solid/liquid aluminum	2.7/2.6	910/960	233/62	933	167
Solid/liquid titanium	4.5/4.0	523/523	21.9/21.9	1941	315
Solid/liquid powder mixture	1.25/1.25	2100/2100	16/16	–	–

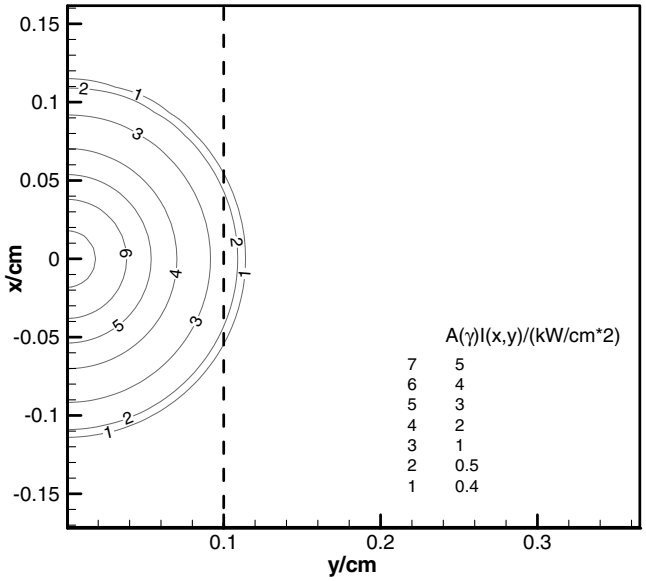

Fig. 2. Distribution of the intensity density of the laser radiation absorbed by the material.

the region is under consideration: $y > 0$. The linear sizes of the calculation domain are: $L_x = 1.5$ cm, $L_y = 3$ cm, $d = 0.2$ cm, $r = 1$ mm, $\alpha = 0$. Radiation power $W = 600$ W, beam radius $\omega_0 = 850$ μm.

In Fig. 2 one can see the distribution of the intensity density of the radiation absorbed by the material $A(\gamma)I(x,y)$. Since the radiation role is reduced, above all, to the initiation of the SHS reactions, the laser beam parameters have been chosen in such a way to direct the largest part of the energy in the Ω_1 – region between the plates. The metal (in regions Ω_2, Ω_3) is under the action of the radiation with the power of about one order lower.

Figs. 3 and 4 show the results of the calculation demonstrating the stationary mode of mixture combustion in the system of coordinates related with the laser beam, as well as the heating and fusion of the metal contacting with the powder. The dotted line indicates the boundary between the powder and metal.

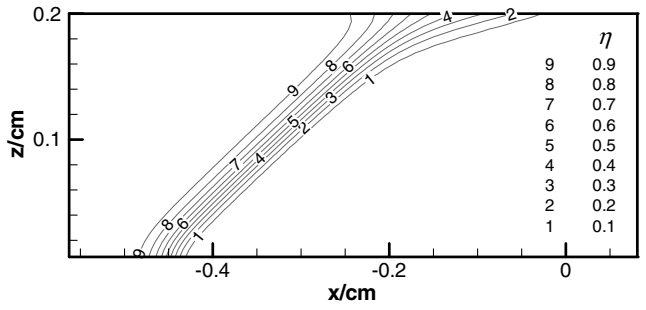

Fig. 3. The isolines of the substance transformation degree η in the combustion wave at $y = 0$.

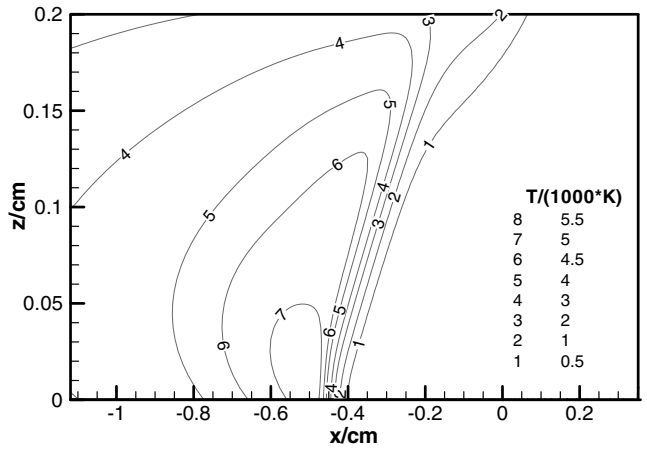

Fig. 4. The isolines of the temperature field in the chemically active region at $y = 0$.

The radiation power of 600 W acting on the joint surface is sufficient only to initiate the chemical reactions in the top part of the joint; the appearing combustion wave penetrates through now the whole joint depth in the self-propagating mode. Fig. 3 presents the isolines of the substance transformation degree in the combustion wave, the width of the chemical reactions zone is 1 mm. The rate of the combustion wave coincides with the speed of beam motion of $V_w = 0.12$ m/s. The combustion front in the XZ plane has an inclination, which characterizes somehow the combustion wave delay in the bottom part of the joint. Recall that the beam axis passes through the coordinate origin and coincides with the OZ axis.

Fig. 4 demonstrates the isolines of the temperature field in the chemically active region. Due to the high thermal conductivity of aluminum, the thermal wave propagates faster in the metal and has time to heat up the bottom part of the joint.

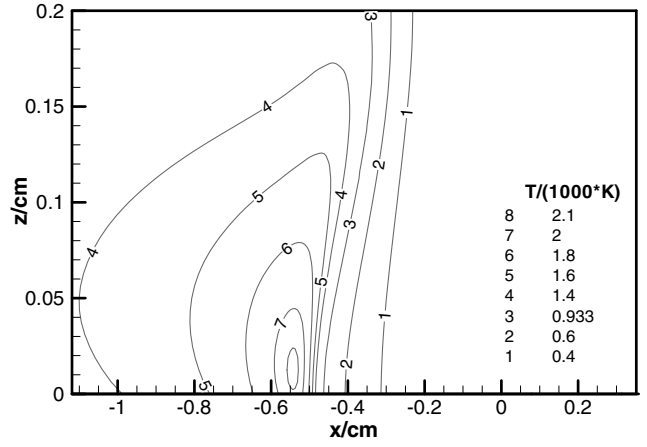

Fig. 5. The isolines of the temperature field at the powder–aluminum boundary.

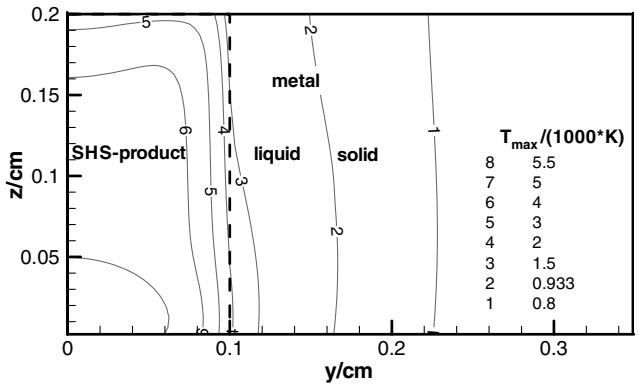

Fig. 6. The isolines of the maximum temperature reached in each point during the whole time of beam scanning, which characterize the shape of the melt bath.

Fig. 5 shows the isolines of the temperature field on the powder and aluminum boundary. The combustion wave propagating in the powder heats up the contact surfaces of the aluminum plates through the whole, above the melting temperature (933 K), which results in the welded joint forming upon the cooling down. The maximum temperature (2121 K) in the aluminum melt is much lower than its boiling point (2723 K). This vindicates that the welding passes in the deep-fusion mode, with no steam–gas region formation.

Fig. 6 presents the isolines of the maximum temperature $T_{\max}(y,z) = \max_{-L_x \leqslant x \leqslant L_x} T(y,z)$, up to which each point of the region was heated during the welding. It is seen that the width of the aluminum fusion zone (melt bath) is 0.6–0.7 mm.

3.3. Welding of heterogeneous metals – aluminum and titanium

The linear sizes of the calculation domain are: $L_x = 1.5$ cm, $L_y = 3$ cm, $d = 0.2$ cm, $r = 0.1$ cm, $\alpha = 0$. Radiation power $W = 2500$ W, beam radius $\omega_0 = 0.1$ cm.

Figs. 7 and 8 show that the combustion wave propagating in the powder heats up the contact surfaces of the plates through the whole, above the melting temperature (933 K for aluminum – Fig. 7, 1941 K for titanium – Fig. 8, correspondingly), which results in the formation of the welded joint upon the cooling down. The maximum temperature in the aluminum melt is 1948 K, in titanium melt – 2436 K. It means that the welding also passes in the deep-fusion mode and the steam–gas region does not form either.

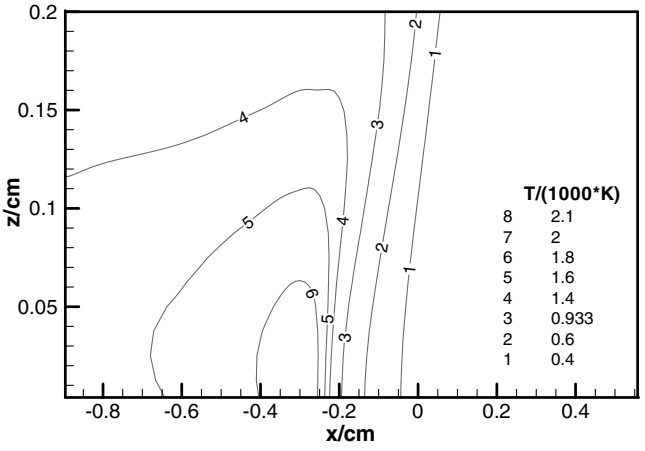

Fig. 7. The isolines of the temperature field on the powder–aluminum boundary.

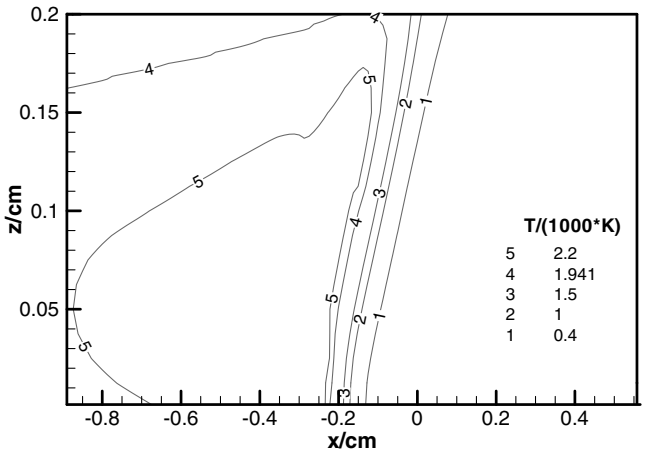

Fig. 8. The isolines of the temperature field at the powder–titanium boundary.

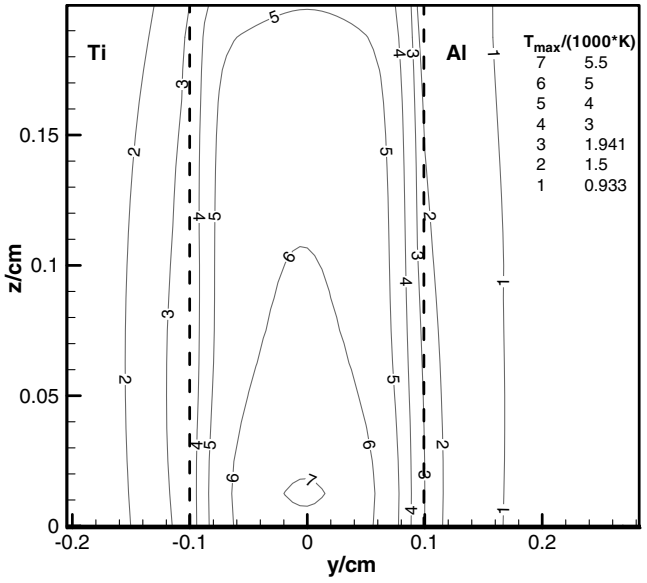

Fig. 9. The isolines of the maximum temperature reached in each point during the whole time of beam scanning, which characterize the shape of the melt bath.

Fig. 9 presents the isolines of the maximum temperature $T_{\max}(y,z) = \max_{-L_x \leqslant x \leqslant L_x} T(y,z)$; each point was heated up to this temperature during the welding. As is seen, titanium is fused to the less depth than aluminum. Fig. 10, which shows the temperature field isolines, demonstrates the heat propagation in the powder and metals in the XY plane at $z = 0.1$ cm. Lower thermal conductivity of titanium (comparing to aluminum) results in the fact that the heat there propagates not that deep, but instead the temperature in the contact with the powder is higher.

3.4. Titanium plates welding

The linear sizes of the calculation domain are: $L_x = 2.5$ cm, $L_y = 3$ cm, $d = 1$ cm, $r = 0.1$ cm, $\alpha = 0$. Radiation power $W = 2500$ W, beam radius $\omega_0 = 0.1$ cm.

Fig. 11 presents that the contact surfaces of the titanium plates are heated through the whole above the melting temperature of 1941 K, which causes the welded joint formation. The maximum temperature reached in the melt is 3054 K. Fig. 12 shows the isolines of the maximum temperature $T_{\max}(y,z) = \max_{-L_x \leqslant x \leqslant L_x} T(y,z)$,

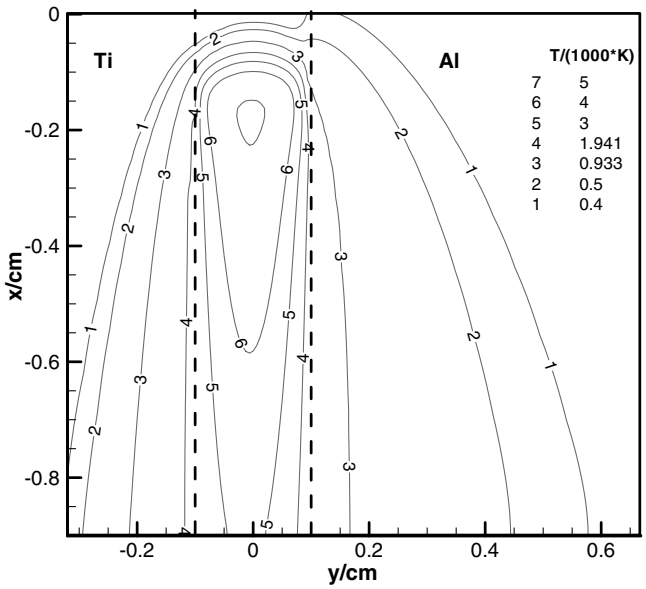

Fig. 10. Propagation of the heat in the powder and metal in the plane $z = 0.1$ cm.

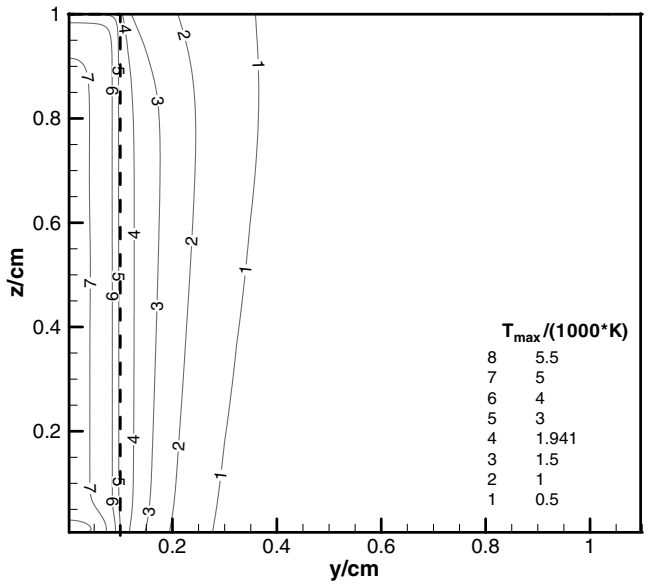

Fig. 12. The isolines of the maximum temperature reached in each point during the whole time of beam scanning, which characterize the shape of the melt bath.

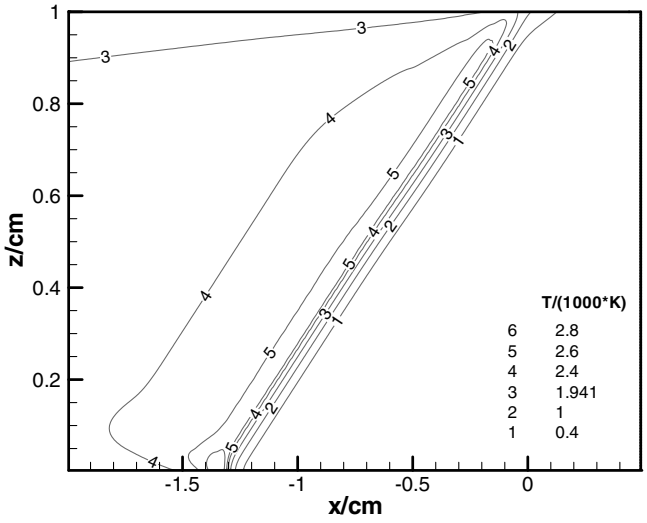

Fig. 11. The isolines of the temperature field at the powder–titanium boundary.

up to which each point of the region was heated during the welding. The depth of titanium fusion is about 0.25 mm.

4. Conclusions

At the moment, the challenge of welding of thick-sheet refractory and heterogeneous metals is topical. In this connection, the potentiality of existing welding technologies turned out to be strongly insufficient. In this paper we propose the theoretical basis of one method of the laser SHS welding with deep fusion. The obtained results are directly related with the challenges of the high-speed welding of aluminum, its alloys, and titanium.

The mathematical model of the high-temperature synthesis of the powder mixture in the narrow clearance between two metal plates, supported by the laser radiation, is offered. The problem of plate joint fusion is solved to realize the fusion welding of them. The model allows to evaluate the needed constants of the generalized kinetics of the chemical reactions in the powder mixture, its thermophysical characteristics, minimum power of the laser beam and the velocity of its scanning.

3D numerical simulation has enabled to determine the thermal modes of the laser ignition and combustion of the mixture, which provide the fusion of the joint details for both homogeneous and heterogeneous metals. The calculations have demonstrated (see the figures) that at low-power laser radiation, metal evaporation is absent. So, the welding passes without any vapor–gas channel. Note that the boiling points for the metals are: 2723 K for aluminum, and 3535 K for titanium. The thickness of the chemical transformations region is about 1 mm, Fig. 3, the rate of the propagating combustion wave does not exceed the rate of beam motion of 0.12 m/s. The powder mixture in the joint region manages to react completely. The effectiveness of joints fusion shows itself in the temperature isolines on the powder and metal interface, Figs. 5, 7, 8, 11, and also in the isolines of the maximal temperature which has ever been reached in the calculation domain points, Figs. 6, 9, 12. For this purpose, the isolines of the metal melting temperatures have been marked in figures: 933 K for aluminum and 1941 K for titanium.

The compound and properties of the powder mixture are of special interest. The calculated stable modes of welding as well as obtained constants of the kinetics of the reaction interaction of the mixture $Q_c = 13.125 \times 10^9$ J/m^3, $k_p = 1.51 \times 10^6$ kg/(s m^3), $p = 0.8$, $E_a = 34$ kJ/mol can be used to calculate the chemical and disperse composition of the powder.

The strength of these welded joints is yet an open question, since no experimental investigations have been done. We can only note that the quality of the welded joints should depend on the compound and properties of the synthesized SHS products. The laser SHS welding is especially effective to weld thick-sheet materials, since it enables to reduce the power of the applied laser radiation.

Acknowledgement

The project has been financially supported by the Russian Foundation for Basic Research (RFBR project codes: 08-08-00249, 06-01-00080).

References

[1] A.G. Merzhanov, I.P. Borovinskaja, A.S. Shteinberg, et al., The method of materials connection, Author's Certificate No. 747661, Bulletin of Inventions No. 26, 1980, p. 55 (in Russian).

[2] M. Ohyanagi, SHS-methods of welded joint of heterogeneous materials, in: M. Koizumi (Ed.), Chemistry of Combustion Synthesis, Mir, Moscow, 1998, pp. 215–231 (in Russian).

[3] V.A. Scherbakov, A.S. Shteinberg, SHS welding of refractory materials, International Journal of Self-Propagation High-Temperature Synthesis 2 (4) (1993) 357–369.

[4] V.A. Scherbakov, Exothermic electric welding of a solid alloy with steel, in: A.E. Sychev (Ed.), Self-Propagating High-Temperature Synthesis: Theory and Practice, Territory, Chernogolovka, 2001, pp. 355–370 (in Russian).

[5] O.B. Kovalev, K.A. Manaichev, Numerical simulation of initiation of SHS reactions in a powder mixture in gap between heat-conducting metal sheets, International Journal of Self-Propagating High-temperature Synthesis 15 (3) (2006) 203–213.

[6] A.G. Merzhanov, Theory and practice of SHS: worldwide state of the art and the newest results, International Journal of Self-Propagating High-temperature Synthesis 2 (2) (1993) 113–158.

[7] A. Makino, Fundamental aspects of the heterogeneous flame in the self-propagating high-temperature synthesis (SHS) process, Progress in Energy and Combustion Science 27 (2001) 1–74.

[8] T.P. Ivleva, A.G. Merzhanov, Three-dimensional modeling of solid-flame chaos, Doklady Physical Chemistry 381 (1–3) (2001) 259–262.

[9] T.P. Ivleva, A.G. Merzhanov, Mathematical simulation of three dimensional spin regimes of gasless combustion, Combustion, Explosion and Shock Waves 38 (1) (2002) 41–48.

[10] A. Biswar, S.K. Roy, K.R. Gurumurthy, N. Prabhu, S. Banerjee, A study of self-propagating high-temperature synthesis of NiAl in thermal explosion mode, Acta Materilia 50 (2002) 757–773.

[11] O.B. Kovalev, V.M. Fomin, The problem of the propagation of a gas-free-combustion wave over the mixture of reacting metal powders, Combustion, Explosion, and Shock Waves 33 (2) (1997) 69–75.

[12] O.B. Kovalev, V.M. Fomin, On the theory of interphase interaction in mixture of reacting metal particles, Combustion, Explosion and Shock Waves 38 (6) (2002) 655–664.

[13] V.V. Andreev, S.S. Vorontsov, O.B. Kovalev, N.A. Pavlov, G.A. Yarygina, Study of ignition and combustion of pyrotechnical compositions under the conditions of intensive heat sink. Lectures of III International Workshop on Unsteady Combustion and Interior Ballistics, vol. 1, Saint Petersburg, 2000, pp. 229–233 (in Russian).

[14] A.A. Samarskii, B.D. Moiseenko, Efficient scheme of through computations for a multidimensional Stefan problem, Zhurnal Vychislitel'noi Matematiki i Matematicheskoi Fiziki 5 (5) (1965) 816–827 (in Russian).

[15] B.M. Budak, E.N. Solov'eva, A.B. Uspenskii, The difference method with factors smoothing for the solution of Stefan problems, Zhurnal Vychislitel'noi Matematiki i Matematicheskoi Fiziki 5 (5) (1965) 828–840 (in Russian).

[16] J.W. Jerome, An operator Newton method for the Stefan problem based on smoothing: a local perspective, Journal of Approximation Theory 62 (3) (1990) 282–296.

[17] M.E. Rose, An enthalpy scheme for Stefan problems in several dimensions, Applied Numerical Mathematics 12 (1–3) (1993) 229–238.